Single-hole dynamics in the t-J model on a square lattice

Michael Brunner, Fakher F. Assaad, and Alejandro Muramatsu
Institut für Theoretische Physik III, Universität Stuttgart, Pfaffenwaldring 57, D-70550 Stuttgart, Federal Republic of Germany
(Received 7 February 2000; revised manuscript received 26 June 2000)

We present quantum Monte Carlo (QMC) simulations for a single hole in a t-J model from $J=0.4t$ to $J=4t$ on square lattices with up to 24×24 sites. The lower edge of the spectrum is directly extracted from the imaginary time Green's function. In agreement with earlier calculations, we find flat bands around $(0,\pm\pi)$, $(\pm\pi,0)$ and the minimum of the dispersion at $(\pm\pi/2,\pm\pi/2)$. For small J, both self-consistent Born approximation and series expansions give a bandwidth for the lower edge of the spectrum in agreement with the simulations, whereas for $J/t>1$, only series expansions agree quantitatively with our QMC results. This band corresponds to a coherent quasiparticle. This is shown by a finite-size scaling of the quasiparticle weight $Z(\vec{k})$ that leads to a finite result in the thermodynamic limit for the considered values of J/t. The spectral function $A(\vec{k},\omega)$ is obtained from the imaginary time Green's function via the maximum entropy method. Resonances above the lowest edge of the spectrum are identified, whose J dependence is quantitatively described by string excitations up to $J/t=2$.

I. INTRODUCTION

Since the pioneering work by Brinkman and Rice[1] (BR) the dynamics of a hole in an antiferromagnet remained as a recurring open problem in condensed-matter physics. After the discovery of high-temperature superconductors[2] and the suggestions by Anderson[3] on the possibility of a non-Fermi-liquid state in those materials, the question whether the quasiparticle weight of a hole vanishes due to the interaction with an antiferromagnetic background became central in the field of strongly correlated fermions.

The BR treatment led to a fully incoherent spectrum in the so-called retraceable path approximation, for an antiferromagnetic Ising-like background, in the limit $J_z\rightarrow 0$. The retraceable path approximation is exact in one[1] and in infinite dimensions[4] but not in two dimensions since contributions of loops (Trugman paths[5]) may lead to a coherent propagation of the hole. Furthermore, for an Ising-like background, it was shown within a Lanczos scheme,[6] that a finite quasiparticle weight is obtained. For the case of physical interest, namely, with a Heisenberg spin background, a large number of numerical methods[7] led to conflicting results. Whereas exact diagonalizations found large quasiparticle peaks at the lower edge of the spectrum,[8] quantum Monte-Carlo (QMC) results were interpreted as leading to a vanishing quasiparticle weight.[9] Since exact diagonalizations are possible only on very small lattices, finite-size scaling cannot be performed reliably. On the other hand, QMC simulations suffered from the minus-sign problem, such that scaling was not possible with reasonable confidence. Further studies based on the self-consistent Born approximation (SCBA)[10–12] gave a finite quasiparticle weight. However, since fluctuations of the spin background are only taken into account in the frame of a spin-wave approximation, the results obtained are not conclusive. Exact results for the supersymmetric point $J=2t$ were obtained by Sorella,[13] that give important benchmarks for any analytical or numerical method (see Sec. III B), but unfortunately, they cannot be rigorously extended to the physical relevant parameter range $J\sim 0.4t$.

Quite recently, the dynamics of a single hole in an antiferromagnetic background became experimentally accessible by angle-resolved photoemission spectroscopy in undoped materials like $Sr_2CuO_2Cl_2$ (Refs. 14 and 15) and $Ca_2CuO_2Cl_2$.[16] The main features observed there are a minimum of the dispersion at $\vec{k}=(\pi/2,\pi/2)$ together with a vanishing of spectral weight beyond this point along the (1,1) direction. The obtained spectra show that the very flat portion around $(\pi,0)$, that in optimally doped materials is almost degenerate with the bottom of the spectrum at $(\pi/2,\pi/2)$,[17] is shifted upwards (in a hole representation) by approximately 300 meV. This contradicts the single-hole spectra found theoretically so far, where essentially the lower edge of the spectrum at $\vec{k}=(\pi/2,\pi/2)$ and $(\pi,0)$ are almost degenerate, such that additional second and third nearest-neighbor hopping terms were suggested,[15,18] that lead to an agreement of the exact diagonalization results with experiments. Such terms were made recently responsible also for the vanishing of spectral weight close to $(\pi/2,\pi/2)$ by reducing the quasiparticle weight.[18,19]

In this paper we present dynamical properties of a single hole in a two-dimensional t-J model on lattices with up to 24×24 sites in the parameter range $0.4\leqslant J/t\leqslant 4$. Results were obtained with a new QMC algorithm, where the spin background is simulated with a loop algorithm[20] and the hole is exactly propagated for a given configuration of the spin background. The lower edge of the spectrum is obtained directly from the asymptotic form of the imaginary time Green's function. The resulting dispersion agrees with previous results obtained within SCBA and series expansions[21] for $J/t<1$, whereas for $J/t>1$ only agreement with series expansions is found. In particular, a flat dispersion is obtained around $\vec{k}=(\pi,0)$ very close in value to the bottom of the band at $\vec{k}=(\pi/2,\pi/2)$, in contrast to the experiments.[14–16] The asymptotics of the imaginary time Green's function delivers also the quasiparticle weight for that band. Finite-size scaling is presented showing that $Z(\vec{k})$ is finite for the parameter range considered, such that the lower edge of the spectrum corresponds to a coherent quasiparticle. Furthermore, our data are consistent with another

exact prediction,[13] namely, that at the supersymmetric point and in the thermodynamic limit, $Z(\vec{Q})/Z(0)=(2m)^2$, where $\vec{Q}=(\pi,\pi)$ is the antiferromagnetic wave vector and m is the staggered magnetization. The spectral function $A(\vec{k},\omega)$ is calculated by analytic continuation with maximum entropy (MaxEnt).[22] Overall agreement is found with exact diagonalizations. At the supersymmetric point, the delta function predicted by Sorella[13] for the wave vector $\vec{k}=(0,0)$ is exactly reproduced. By extracting the contribution of the quasiparticle from the imaginary time Green's function, a resonance above the quasiparticle band is made evident, that together with the lower edge of the spectrum scales as $J^{2/3}$, in agreement with the string picture[23] used to described the excitations for a hole in an antiferromagnetic Ising background. Remarkably, also the prefactors of the corresponding Airy functions are needed in order to properly describe the distance between the resonance and the quasiparticle band.

The paper is organized as follows. Section II describes the model, a canonical transformation that leads to a bilinear form in spinless fermions interacting with $S=\frac{1}{2}$ pseudospins, and the algorithm. Since the Hamiltonian for the transformed *t-J* model is bilinear in fermions (the holes), their propagation can be calculated exactly given a pseudospin configuration. In Sec. III the results are discussed. Section III A describes the lower edge of the spectrum and how it is obtained. In Sec. III B the results for the quasiparticle weight are shown. Section III C describes the spectral function $A(\vec{k},\omega)$ and the string excitations. Finally, the conclusions are given in Sec. IV.

II. THE MODEL AND THE ALGORITHM

The *t-J* model is a suitable one to simulate the dynamics of a single hole in an antiferromagnet. On the one side, it can be obtained from the Hubbard model in the large coupling limit, which at half-filling leads to the Heisenberg antiferromagnet. On the other side, it is the relevant one to simulate the cuprates, as shown by Zhang and Rice,[24] and hence, to compare with experiments.[14–16] Its Hamiltonian is

$$H_{t\text{-}J}=-t\sum_{\langle i,j\rangle,\sigma}\tilde{c}^{\dagger}_{i,\sigma}\tilde{c}_{j,\sigma}+J\sum_{\langle i,j\rangle}(\vec{S}_i\cdot\vec{S}_j-\tfrac{1}{4}\tilde{n}_i\tilde{n}_j), \qquad (1)$$

where $\tilde{c}^{\dagger}_{i,\sigma}$ are projected fermion operators $\tilde{c}^{\dagger}_{i,\sigma}=(1-c^{\dagger}_{i,-\sigma}c_{i,-\sigma})c^{\dagger}_{i,\sigma}$, $\tilde{n}_i=\Sigma_{\alpha}\tilde{c}^{\dagger}_{i,\alpha}\tilde{c}_{i,\alpha}$, $\vec{S}_i=(1/2)\Sigma_{\alpha,\beta}c^{\dagger}_{i,\alpha}\vec{\sigma}_{\alpha,\beta}c_{i,\beta}$, and the sum runs over nearest neighbors only. In order to render Eq. (1) a bilinear form in fermionic operators, we perform a canonical transformation:[25]

$$c^{\dagger}_{i\uparrow}=\gamma_{i,+}f_i-\gamma_{i,-}f^{\dagger}_i, \quad c^{\dagger}_{i\downarrow}=\sigma_{i,-}(f_i+f^{\dagger}_i), \qquad (2)$$

where $\gamma_{i,\pm}=(1\pm\sigma_{i,z})/2$ and $\sigma_{i,\pm}=(\sigma_{i,x}\pm i\sigma_{i,y})/2$. The spinless fermion operators fulfill the canonical anticommutation relations $\{f^{\dagger}_i,f_j\}=\delta_{i,j}$, and $\sigma_{i,a}$, $a=x$, y, or z are the Pauli matrices. The Hamiltonian becomes

$$\tilde{H}_{t\text{-}J}=+t\sum_{\langle i,j\rangle}P_{ij}f^{\dagger}_i f_j+\frac{J}{2}\sum_{\langle i,j\rangle}\Delta_{ij}(P_{ij}-1), \qquad (3)$$

where $P_{ij}=(1+\vec{\sigma}_i\cdot\vec{\sigma}_j)/2$, $\Delta_{ij}=(1-n_i-n_j)$ and $n_i=f^{\dagger}_i f_i$. The constraint to avoid doubly occupied states transforms to the conserved and holonomic constraint $\Sigma_i\gamma_{i,-}f^{\dagger}_i f_i=0$. This constraint simply means that a spinless fermion and a pseudospin $\downarrow$ are not allowed to sit on the same site. The main advantage of this formulation of the *t-J* model is the fact that fermions only appear in bilinear form in contrast to the original formulation of the *t-J* model (1).

In order to obtain the dynamics of the hole, we calculate the one-particle Green's function for spin up,

$$G(i-j,\tau)=-\langle T\tilde{c}_{i,\uparrow}(\tau)\tilde{c}^{\dagger}_{j,\uparrow}\rangle=-\langle Tf^{\dagger}_i(\tau)f_j\rangle, \qquad (4)$$

where T corresponds to the time-ordering operator. We first perform a Trotter decomposition of the partition sum

$$\mathbf{Z}=\mathrm{Tr}\exp(-\beta H)=\mathrm{Tr}\lim_{M\to\infty}\{\exp[-(\beta/M)H^1]\times\exp[-(\beta/M)H^2]\ldots\exp[-(\beta/M)H^{2d}]\}^M, \qquad (5)$$

where the Hamilton operator is split up in $2d$ (d is the dimension of the system) terms $H^1,H^2,\ldots,H^{2d}$. These terms can be handled easily, as they only consist of disconnected two-site terms. At all intermediate time steps, complete sets of spin states are inserted. Then the Green's function (4) transforms as (we consider the case $d=1$):

$$\begin{aligned}G(i-j,-\tau)&=\frac{\sum_{\sigma_{(1,1)}}\langle v|\otimes\langle\sigma_{(1,1)}|e^{-(\beta-\tau)\tilde{H}_{t\text{-}J}}f_j e^{-\tau\tilde{H}_{t\text{-}J}}f^{\dagger}_i|\sigma_{(1,1)}\rangle\otimes|v\rangle}{\sum_{\sigma_{(1,1)}}\langle\sigma_{(1,1)}|e^{-\beta\tilde{H}_{t\text{-}J}}|\sigma_{(1,1)}\rangle}\\&=\sum_{\vec{\sigma}}P(\vec{\sigma})\frac{\langle v|f_j e^{-\Delta\tau\tilde{H}^1(\sigma_{(n,1)},\sigma_{(n-1,2)})}\ldots e^{-\Delta\tau\tilde{H}^2(\sigma_{(1,2)},\sigma_{(1,1)})}f^{\dagger}_i|v\rangle}{\langle\sigma_{(n,1)}|e^{-\Delta\tau\tilde{H}^1_{t\text{-}J}}|\sigma_{(n-1,2)}\rangle\ldots\langle\sigma_{(1,2)}|e^{-\Delta\tau\tilde{H}^2_{t\text{-}J}}|\sigma_{(1,1)}\rangle}+\mathcal{O}(\Delta\tau^2)\\&=\sum_{\vec{\sigma}}P(\vec{\sigma})G(i,j,\tau,\vec{\sigma})+\mathcal{O}(\Delta\tau^2).\end{aligned} \qquad (6)$$

Here $m\Delta\tau=\beta$, $n\Delta\tau=\tau$, $\Delta\tau t\ll 1$, and $\exp[-\Delta\tau\tilde{H}(\sigma_1,\sigma_2)]$ is the evolution operator for the holes, given the spin configuration (σ_1,σ_2). In the case of single-hole dynamics, $|v\rangle$ is the vacuum state for holes, and

$$P(\vec{\sigma})=\frac{\langle\sigma_{(1,1)}|e^{-\Delta\tau\tilde{H}^1_{t\text{-}J}}|\sigma_{(m,2)}\rangle\langle\sigma_{(m,2)}|e^{-\Delta\tau\tilde{H}^2_{t\text{-}J}}|\sigma_{(m,1)}\rangle\ldots\langle\sigma_{(1,2)}|e^{-\Delta\tau\tilde{H}^2_{t\text{-}J}}|\sigma_{(1,1)}\rangle}{\sum_{\vec{\sigma}}\langle\sigma_{(1,1)}|e^{-\Delta\tau\tilde{H}^1_{t\text{-}J}}|\sigma_{(m,2)}\rangle\langle\sigma_{(m,2)}|e^{-\Delta\tau\tilde{H}^2_{t\text{-}J}}|\sigma_{(m,1)}\rangle\ldots\langle\sigma_{(1,2)}|e^{-\Delta\tau\tilde{H}^2_{t\text{-}J}}|\sigma_{(1,1)}\rangle} \tag{7}$$

is the probability distribution of a Heisenberg antiferromagnet for the configuration $\vec{\sigma}$, where $\vec{\sigma}$ is a vector containing all intermediate states $(\sigma_{(1,1)},\sigma_{(m,2)},\ldots,\sigma_{(n,2)},\sigma_{(n,1)},\ldots,\sigma_{(1,1)})$. The sum over spins is performed in a very efficient way by using a world-line loop algorithm[20] for a Heisenberg antiferromagnet with discretized imaginary time. In general we have $\Delta\tau=0.05$, such that the extrapolation to $\Delta\tau=0$ leads to values of the observables within the statistical error bars. The inverse temperature β is taken such that the energy is well converged ($\beta J\geqslant 20$ for 16×16 and $\beta J=30$ for 24×24 sites), and therefore, the data correspond to the ground state. As the evolution operator for the holes is a bilinear form in the fermion operators, $G(i,j,\tau,\vec{\sigma})$ can be calculated exactly, in contrast to a direct implementation in the loop algorithm,[26,27] where fermion paths are sampled stochastically. $G(i,j,\tau,\vec{\sigma})$ contains a sum over all possible fermion paths between $(i,0)$and (j,τ). The numerical effort to calculate $G(i,j,\tau,\vec{\sigma})\forall\, i,\tau$ scales as $N\tau$, where N is the number of lattice points in space. Therefore, the present method is more efficient for large systems than, e.g., projector algorithms for the Hubbard model, that scale with the system size cubed.

With the representation of Eq. (3), the propagation of down-spin electrons cannot be easily considered, since the operators $\sigma_{i,\pm}$ cut world lines. This is certainly not a problem for finite-size systems, where SU(2) spin symmetry is conserved. Since $P(\vec{\sigma})$ is the probability distribution for the quantum antiferromagnet, the algorithm does not suffer from sign problems on bipartite lattices and nonfrustrating magnetic interactions in any dimension.

We now address the explicit calculation of $G(i,j,\tau,\sigma)$, the Green's function for the fermions given a spin background. In a first step, we introduce additional complete sets of single fermion states in the numerator of Eq. (6), such that $G(i,j,\tau,\vec{\sigma})$ becomes

$$\begin{aligned}G(i,j,\tau,\vec{\sigma})=&\langle v|f_j\Bigg(\sum_{\vec{l}}|f_{l_{(n,1)}}\rangle\frac{\langle f_{l_{(n,1)}}|e^{-\Delta\tau\tilde{H}^1(\sigma_{(n,1)},\sigma_{(n-1,2)})}|f_{l_{(n-1,2)}}\rangle}{\langle\sigma_{(n,1)}|e^{-\Delta\tau H^1_{t\text{-}J}}|\sigma_{(n-1,2)}\rangle}\\&\times\frac{\langle f_{l_{(n-1,2)}}|e^{-\Delta\tau\tilde{H}^2(\sigma_{(n-1,2)},\sigma_{(n-1,1)})}|f_{l_{(n-1,1)}}\rangle}{\langle\sigma_{(n-1,2)}|e^{-\Delta\tau H^2_{t\text{-}J}}|\sigma_{(n-1,1)}\rangle}\ldots\times\ldots\frac{\langle f_{l_{(1,2)}}|e^{-\Delta\tau\tilde{H}^2(\sigma_{(1,2)},\sigma_{(1,1)})}|f_{l_{(1,1)}}\rangle}{\langle\sigma_{(1,2)}|e^{-\Delta\tau H^2_{t\text{-}J}}|\sigma_{(1,1)}\rangle}\langle f_{l_{(1,1)}}|\Bigg)f_i^\dagger|v\rangle\\=&\sum_{\vec{l}}[\delta^j_{l_{(n,1)}}U^1(\sigma_{(n,1)},\sigma_{(n-1,2)})^{l_{(n,1)}}_{l_{(n-1,2)}}U^2(\sigma_{(n-1,2)},\sigma_{(n-1,1)})^{l_{(n-1,2)}}_{l_{(n-1,1)}}\ldots U^2(\sigma_{(1,2)},\sigma_{(1,1)})^{l_{(1,2)}}_{l_{(1,1)}}\delta_i^{l_{(1,1)}}],\end{aligned} \tag{8}$$

where the sum $\Sigma_{\vec{l}}$ runs over all possible intermediate one-particle states in the fermionic Hilbert space $\{|f_l\rangle\}$. The propagators $\langle f_{l_p}|e^{-\Delta\tau\tilde{H}(\sigma_p,\sigma_{p-1})}|f_{l_{p-1}}\rangle/\langle\sigma_p|e^{-\Delta\tau H}|\sigma_{p-1}\rangle$ are only nonzero, when l_p and l_q belong to the same plaquette. As the fermions only appear in bilinear form, these propagators can easily expressed by $N\times N$ matrices (N is the size of the system). The entries of these matrices $U^{1,2}(\sigma_p,\sigma_q)$ are nonzero only at the positions that correspond to a plaquette in the checkerboard breakup, and therefore only two positions in the matrices per line are nonzero. The possible values for these entries are given in Table I. As we are only interested in the Hilbert space with no double occupancy, we have to enforce the constraint at one single position of the propagation by projecting out the fermionic states that do not respect the constraint. We do so at $\tau=0$ corresponding to the first propagation.

As discussed above, we use a loop algorithm with discretized imaginary time, to sample the probability distribution $P(\vec{\sigma})$ of the Heisenberg antiferromagnet, which leads to a systematic error $\mathcal{O}(\Delta\tau^2)$. The loop algorithm[20] has been extended to work in continuous time,[28] where this systematic error is eliminated. However, in our case, it is not sufficient to formulate the spin dynamics in continuous time, but we have to reformulate the algorithm such that the propagation of the fermion takes place in continuous time synchronously. The following problems will arise, when a continuous time loop algorithm is used to sample $P(\vec{\sigma})$:

(i) the $N\times N$ matrices $U(\sigma_p,\sigma_q)$ to propagate the one-particle states are no longer sparse matrices formed by 2×2 matrices only, and they have to be recalculated from scratch for every spin configuration.

(ii) In the case of continuous time the average number of matrices $U(\sigma_p,\sigma_q)$ for the propagation of the fermions is $\sim\beta JN$ as opposed to $\sim\beta/\Delta\tau$ for discretized time. At least for large systems the number of matrices is therefore much larger for continuous time than for discrete time. Both points (i) and (ii) will reduce the efficiency of the algorithm drastically.

TABLE I. Contributions for the propagation of the hole on one plaquette. The first column shows the weight for a propagation where the hole stays on the same site x, whereas in the second column the weight corresponds to the propagation to the adjacent site. The third column represents the spin background on the plaquette.

$x\rightarrow x$	$x+\boldsymbol{\delta}\rightarrow x$	Spin configuration
0	0	$\downarrow\ \downarrow$ / $\downarrow\ \downarrow$
$\cosh(\Delta\tau t)$	$-\sinh(\Delta\tau t)$	$\uparrow\ \uparrow$ / $\uparrow\ \uparrow$
$\dfrac{\cosh(\Delta\tau t)}{\exp(\Delta\tau J/2)\cosh(\Delta\tau J/2)}$	0	$\uparrow\ \downarrow\downarrow\ \uparrow$ / $\uparrow\ \downarrow'\downarrow\ \uparrow$
0	$\dfrac{\sinh(\Delta\tau t)}{\exp(\Delta\tau J/2)\sinh(\Delta\tau J/2)}$	$\downarrow\ \uparrow\uparrow\ \downarrow$ / $\uparrow\ \downarrow'\downarrow\ \uparrow$

The one-particle spectral function

$$A(\vec{k},\omega)=\sum_{f,\sigma}|\langle f,N-1\,|c_{\vec{k},\sigma}|\,0,N\rangle|^2\,\delta(\omega-E_0^N+E_f^{N-1}) \tag{9}$$

is connected with the Green's function in imaginary time at $T=0$, by the spectral theorem

$$G(\vec{k},\tau)=\int_{-\infty}^{\infty}d\omega\,\frac{\exp(-\tau\omega)}{\pi}A(\vec{k},\omega). \tag{10}$$

Here $|\,0,N\rangle$ is the ground state at half-filling with energy E_0^N and $|\,f,N-1\rangle$ are states in the $N-1$ particle Hilbert space with energy E_f^{N-1}. We perform the inversion of Eq. (10), that due to the statistical errors of $G(\vec{k},\tau)$ is an extremely ill-posed problem, by means of MaxEnt, where the $A(\vec{k},\omega)$ obtained is the one that maximizes the probability $P(A|G)$, given the Green's function $G(\vec{k},\tau)$. Correlations in the imaginary time data were taken into account by considering the covariance matrix. The default model for the MaxEnt analysis is taken flat without prior knowledge. Details about MaxEnt can be found in the comprehensive review article by Gubernatis and Jarrell.[22]

Finally, we would like to stress, that part of the dynamical data presented below were obtained without use of MaxEnt but directly extracted from the imaginary time Green's function. This is possible due to the high statistics and stability attainable with the present algorithm. The slowest decaying exponential, that corresponds to the excitation with lowest energy can be extracted simply by fitting the tail of the Green's function at large values of τ. This leads to the value of the excitation and its corresponding weight, as shown in Secs. III A and III B. Furthermore, in connection with MaxEnt, the next higher excitation can be obtained by subtracting the contribution from the lowest one from the Green's function. This procedure is discussed in Sec. III C.

III. RESULTS

We concentrate in the following on three aspects of the dynamics of a single hole in a Heisenberg antiferromagnet.

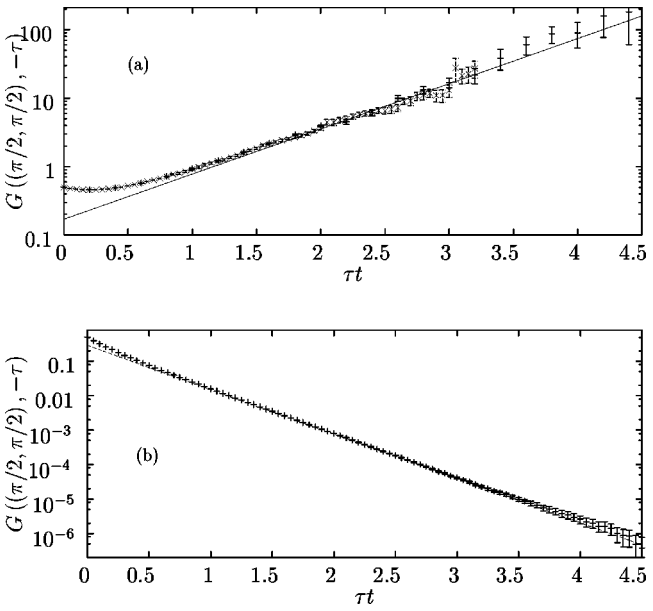

FIG. 1. The energy of the lowest excitation is extracted from the imaginary time asymptotics of the Green's function, as indicated by the dotted line for (a) $J=0.4t$ (both for $\Delta\tau=0.2$ and $\Delta\tau=0.05$) and (b) $J=2t$ ($\Delta\tau=0.05$) in a 16×16 lattice.

First we consider in Sec. III A the lower edge of the spectrum. This is a quantity that can be obtained by several other methods, including various Monte-Carlo algorithms, such that the relative accuracy of each one and the region in parameter space, where each method gives best results, can be assessed. In our case, this quantity is obtained from the asymptotic behavior of the one-particle Green's function in imaginary time. However, not only the energy but also the weight of such an excitation can be extracted from the asymptotics, leading to the quasiparticle weight, as discussed in Sec. III B. The present algorithm is up to now the only one capable of extracting this information for the t-J model free of approximations on large lattices (in general up to 16×16 and for $J/t=2$ up to 24×24 sites). For small lattice sizes, the results can be compared with exact diagonalizations, whereas for large systems only comparisons with approximate methods like SCBA can be made. Finally, the whole spectrum is considered in Sec. III C, where the spectral function $A(\vec{k},\omega)$ is discussed. Using the information from the lower edge of the spectrum, a resonance above the quasiparticle band is identified, which is very well described as a string excitation.

A. The lower edge of the spectrum

The accuracy and stability of the data allow, in our case, to obtain the lower edge of the spectrum directly from the slope of the one-particle Green's function as a function of imaginary time τ, for large values of τ. Figure 1 shows the asymptotics in imaginary time for two values of the coupling constant, showing that the most accurate results are obtained, when $J/t=2$. $J/t=0.4$ is the smallest coupling, where such a procedure can be applied. In order to check the results obtained at the smallest coupling, we made additional calculations at $\Delta\tau t=0.2$ (all other calculations are done at $\Delta\tau t$

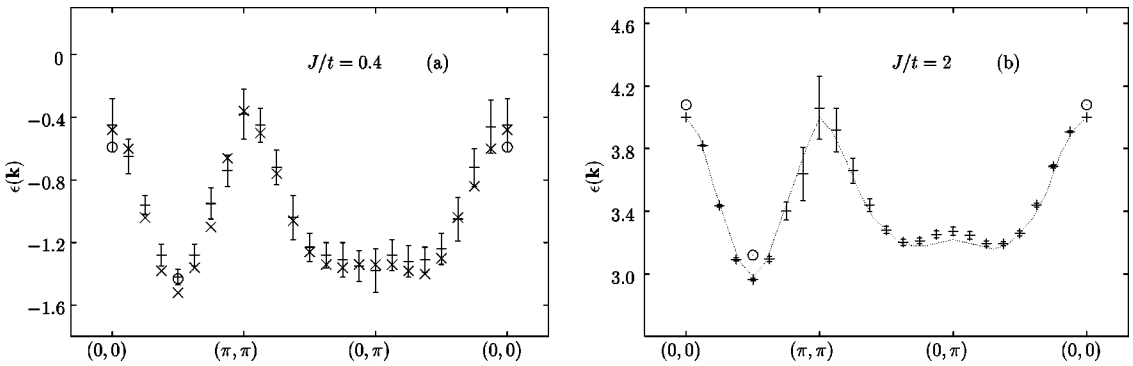

FIG. 2. Lower edge of the spectrum along the symmetry lines of the Brillouin zone for (a) $J/t=0.4$ and (b) $J/t=2$ in a 16×16 lattice. Comparisons are made with VMC (circles), GFMC for $J/t=0.4$ ($\times$), and series expansion (Ref. 21) for $J/t=2$ (dotted line).

$=0.05$), where larger values of τt can be reached. The resulting Green's functions are the same within the error bars, indicating a small $\Delta\tau$ effect.

Figure 2 shows the lower edge of the spectrum for $J/t=0.4$ and $J/t=2$ in a 16×16 sites system. The energies are displayed with respect to the ground-state energy of the Heisenberg antiferromagnet. The results are compared with variational Monte Carlo (VMC),[29] Green's function Monte Carlo (GFMC),[30] and series expansions,[21] whenever data is available. At $J/t=0.4$ [Fig. 2(a)], where our results are most affected by fluctuations, we observe good agreement with GFMC. The behavior of the statistical error is similar in both methods, with larger fluctuations around $\vec{k}=(0,0)$ and (π,π). Around $\vec{k}=(\pi,0)$ our results show somewhat larger fluctuations. For $J/t=0.4$ VMC,[29] also appears to be very accurate concerning the lower edge. When its energies are compared to our calculations and the GFMC technique, we find that their energies are within the error bars of the exact QMC calculations. At $\vec{k}=(0,0)$, the variational result is at the lower edge of the error bars of our calculation, and have the smallest statistical error of all three approaches. At this specific k point both GFMC and our approach have large fluctuations before the state with lowest energy is clearly reached. As mentioned above, additional calculations with $\Delta\tau t=0.2$ were performed, in order to check the results obtained, without observing significant changes.

Figure 2(b) shows that at $J/t=2$, where our algorithm leads to much more accurate results, the variational results are too high in energy, but still close to our numerically exact ones. For values of $J/t\geqslant1$, additional results from series expansions[21] are available. At $J/t=2$ we observe in general a very good agreement. Around $(\pi,0)$ we see that series expansions slightly underestimate the energy of the hole. The general features of the lower edge are not substantially modi-

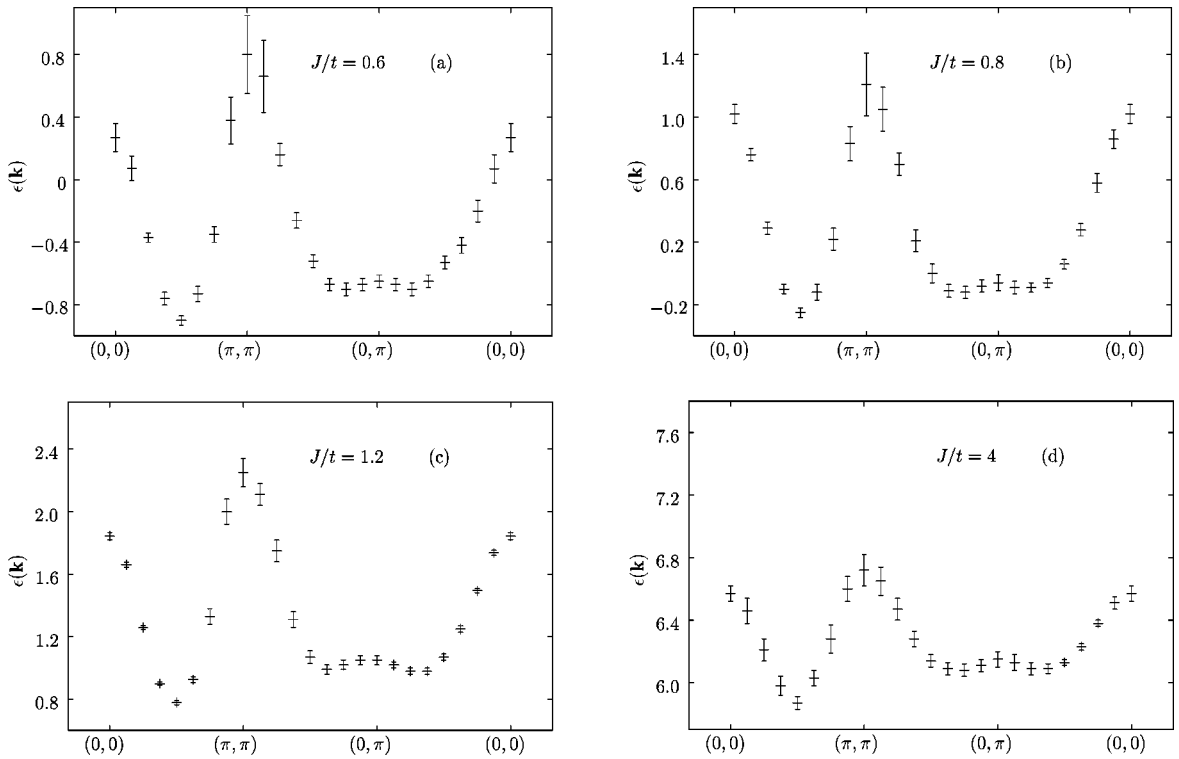

FIG. 3. Lower edge of the spectrum along the symmetry lines of the Brillouin zone for (a) $J/t=0.6$, (b) $J/t=0.8$, (c) $J/t=1.2$, and (d) $J/t=4$ in a 16×16 lattice.

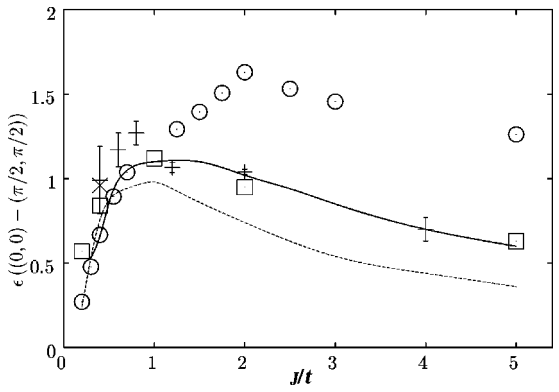

FIG. 4. Bandwidth of the lower edge as a function of J/t. $\epsilon(0,0)-\epsilon(\pi/2,\pi/2)$ in a 16×16 lattice compared with exact diagonalization (4×4 sites, open circles), GFMC (cross), VMC (open boxes), SCBA (dashed line), and series expansions (full line).

fied when going from $J/t=0.4$ to $J/t=4$. This is shown in Fig. 3, where the only changes observed are an overall shift in energy with respect to the Heisenberg antiferromagnet and a change in the bandwidth. The shift in energy can be followed by considering the dependence of $\epsilon(\pi/2,\pi/2)$ on J/t. This dependence is rather accurately described by $\epsilon(J/t)/t=-3.28+a_1(J/t)^{2/3}$, where a_1 is the first eigenvalue of the dimensionless Airy equation (see Fig. 13 in Sec. III C). Such a scaling of the hole energies is found in the t-J_z model in the continuum limit for small values of J_z,[23,10,12] when loops along the path of the hole are disregarded. In that case, the constant is $-2\sqrt{z-1}$, where z is the coordination number. The resulting string picture gives an accurate description of the lowest excitations close to $\vec{k}=(\pi/2,\pi/2)$. As will be shown in Sec. III C, the next higher excitation can also be described by the string picture.

Figure 4 shows the bandwidth obtained in our simulations compared with exact diagonalizations,[33] GFMC,[30] SCBA,[11,12] VMC,[29] and series expansions.[21] For $J/t<0.8$ good agreement is found among all methods, whereas for larger values of J, only series expansions and VMC agree with our data. This, and the fact that the string picture gives a good representation of the lowest lying states, suggest that a perturbation expansion as performed in series expansions can be used to interpret the distinctive features of the lower edge. In particular, the flat band observed around $\vec{k}=(\pi,0)$ and the fact that the degeneracy between this point and $\vec{k}=(\pi/2,\pi/2)$, suggested by some approaches,[31] is clearly lifted, as shown by our simulation, are very well reproduced by series expansions. The flat bands can be well observed for all considered values of J/t, when considering the lower edge (Figs. 2 and 3) and the complete spectral function (Fig. 11). Our data clearly show for $J/t\geq0.6$, that the neighboring points of $\vec{k}=(\pi,0)$ are generally slightly higher in energy. The band in this area does not seem to be completely flat, but it changes its curvature with local minima of the dispersion at the points (π,δ) and $(\pi-\delta,0)$, when going along the (1,0) and (0,1) directions, respectively, with the *caveat* that they are well defined beyond the error bars only for $J/t>1$. In all the cases we find $\delta\approx0.3\pi$. This region with a very flat band spans an extremely large area in the Brillouin zone.

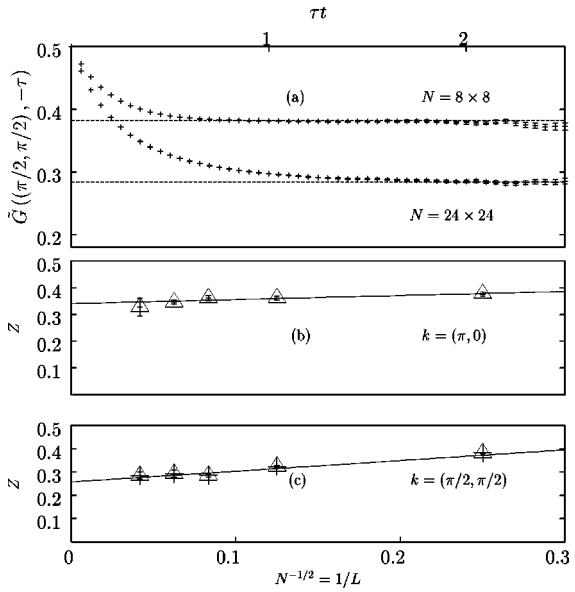

FIG. 5. (a) Extrapolation of $\tilde{G}(\vec{k},-\tau)\equiv G(\vec{k},-\tau)\exp[(\epsilon_k-\epsilon_0)\tau]$ for $N=8\times8$ and 24×24 at $J/t=2$. Finite-size scaling for (b) $\vec{k}=(\pi/2,\pi/2)$ and (c) $\vec{k}=(\pi,0)$.

A flat band on a similarly wide region in the Brillouin zone around $\vec{k}=(\pi,0)$ is also observed in photoemission spectroscopy of cuprates close to the Fermi energy in the optimally doped compounds. As doping is reduced, that portion of the spectrum opens a pseudogap and weight is transferred to higher energies,[17] until in the undoped materials, this portion is about $2J$ (≈300 meV) above the minimum at $\vec{k}=(\pi/2,\pi/2)$.[14–16] The energy difference between the points $\vec{k}=(\pi/2,\pi/2)$ and $\vec{k}=(\pi,0)$ is in our simulation about $\Delta=(0.25\pm0.10)t$ ($\approx J/2$ for $J=0.4t$). The rather large error corresponds mainly to $J/t<1$. No significant dependence on J/t can be observed in the whole range under consideration, in contrast to the results from SCBA and series expansions. However, it could be that the J dependence is masked in our case by large fluctuations, taking into account that the variations observed for this quantity by SCBA and series expansions are much smaller than the one observed for the bandwidth. SCBA (Ref. 11) gives values ranging from $0.17t$ ($J/t=1$) to $0.12t$ ($J/t=4$), that are smaller than the values we obtain. On the other hand, series expansions[21] obtain val-

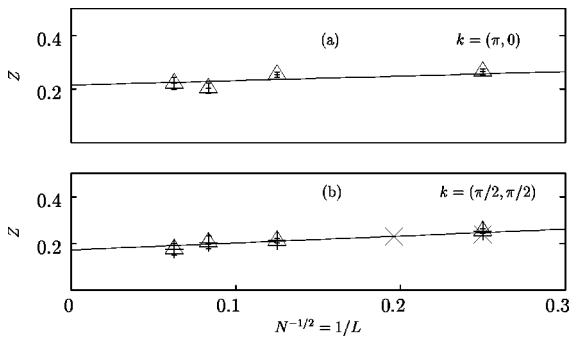

FIG. 6. Finite-size scaling of $Z(\vec{k})$ at $J/t=0.6$ for (a) $\vec{k}=(\pi/2,\pi/2)$ and (b) $\vec{k}=(\pi,0)$. The crosses are values from exact diagonalization results (Refs. 33 and 32).

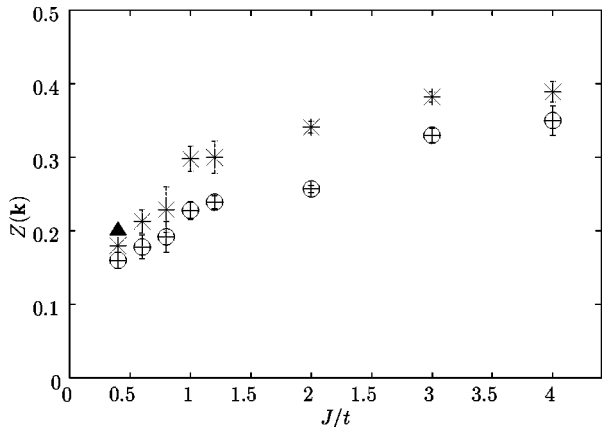

FIG. 7. Quasiparticle weight as a function of J/t for $\vec{k}=(\pi/2,\pi/2)$ (circles) and $\vec{k}=(\pi,0)$ ($\times$). The result from exact diagonalization (Ref. 33) in a 4×4 lattice is given by the triangle. The data points at $J/t=0.4$ are considered as an upper bound.

ues between $0.15t$ at $J/t=1$ and $0.25t$ at $J/t=2.5$. The values obtained by series expansions are consistent with our results for large values of J/t.

B. The quasiparticle weight

The quasiparticle weight is the weight of the exponential with the slowest decay, that is the exponential that determines the lower edge of the spectrum. This weight is

$$Z(\vec{k})=\lim_{-\tau\to\infty} G(-\tau,\vec{k})\exp[(\epsilon_{\vec{k}}-\epsilon_0)\tau]. \qquad (11)$$

In the following we focus on the thermodynamic limit of $Z(\vec{k})$ for the wave vectors $\vec{k}=(\pi,0)$ and $\vec{k}=(\pi/2,\pi/2)$. Figures 5 and 6 show the finite-size scaling on these two points for $J/t=2$ and $J/t=0.6$, respectively. For both k and J values, an appreciable quasiparticle weight is obtained, demonstrating that the lower edge of the spectrum describes the band of a coherent quasiparticle. The determination of the

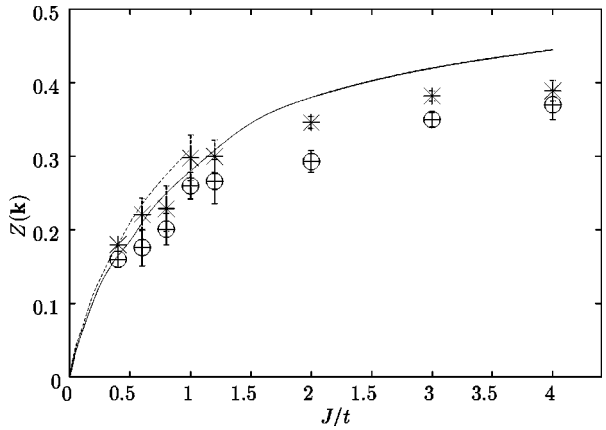

FIG. 8. Quasiparticle weight as a function of J/t for $\vec{k}=(\pi/2,\pi/2)$ (circles) and $\vec{k}=(\pi,0)$ ($\times$) in a 16×16 lattice (the values for $J/t=0.4$ are an upper bound only). We compare our result with SCBA, where the dashed line corresponds to the quasiparticle weight for $\vec{k}=(\pi,0)$ and the full line corresponds to $\vec{k}=(\pi/2,\pi/2)$. The data points were taken from Ref. 11.

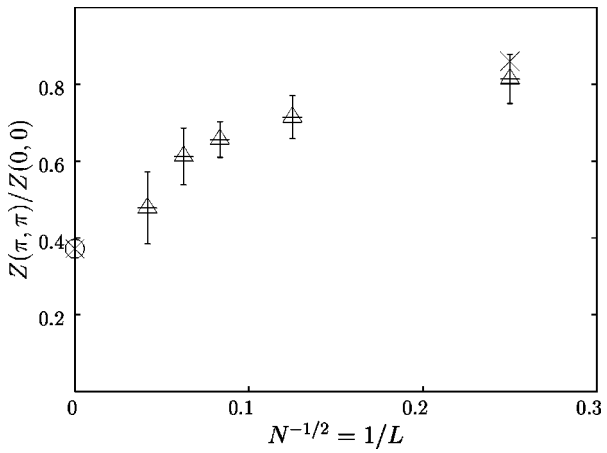

FIG. 9. Finite-size scaling for the quasiparticle weight at $\vec{Q}=(\pi,\pi)$ for $J/t=2$. The cross in the thermodynamic limit is $(2m)^2$, m being the staggered magnetization.

quasiparticle weight is only accurate for $J/t\geq0.6$. Below that value, the quality of the data is less satisfactory (see Fig. 1) and, for $J/t=0.4$ the value presented can be taken only as an upper bound. The size dependence of $Z(\pi/2,\pi/2)$ and $Z(\pi,0)$ is not very large and scales linearly with the inverse linear size of the system for $J/t\geq0.6$, in agreement with SCBA.[11] The size dependence at $(\pi/2,\pi/2)$ is systematically larger than at $(\pi,0)$. The sizes considered are $L\times L$, with $L=16$, 12, 8, and 4. At $J/t=2$ we use additionally a 24×24 lattice. Values from exact diagonalization[32,8,33] were included when available.

Figure 7 shows that the extrapolated quasiparticle weight increases with J/t both for $\vec{k}=(\pi,0)$ and $\vec{k}=(\pi/2,\pi/2)$. At $J/t=4$ the quasiparticle reaches about 80% of its maximal value. The changes of the quasiparticle weight with J/t are small when $J/t\geq1$ and the slope becomes steeper for smaller values. Estimates of the quasiparticle weight were given both by VMC (Ref. 29) and SCBA,[11] the difference being rather small. The general trend is that VMC overestimates it at

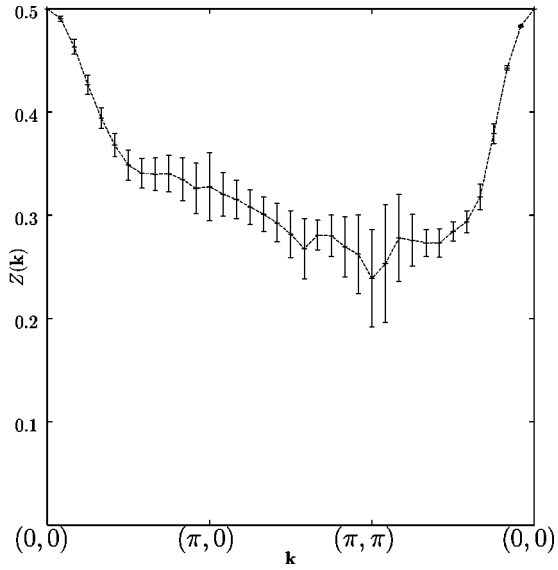

FIG. 10. $Z(\vec{k})$ along the symmetry lines in the Brillouin zone for $J/t=2$ in a 24×24 lattice.

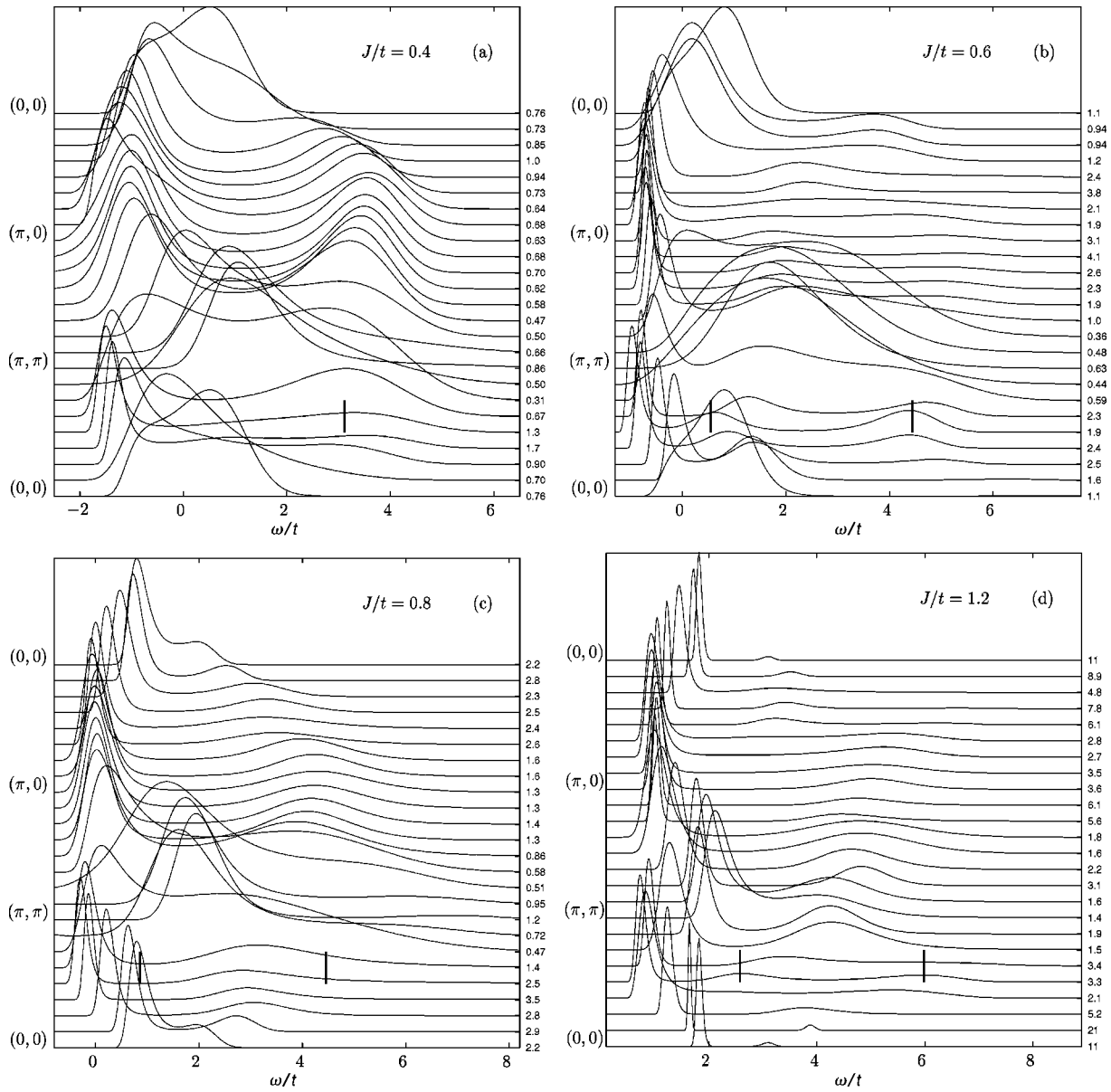

FIG. 11. Spectral function for a 16×16 system and (a) $J/t=0.4$, (b) 0.6, (c) 0.8, (d) 1.2, (e) 2, and (f) 4. The vertical lines indicate resonances above the quasiparticle peak at $\vec{k}=(\pi/2,\pi/2)$ as obtained in Sec. III C, Fig. 16.

small J whereas SCBA overestimates it at large J. For definiteness we compare our results with SCBA for a 16×16 system in Fig. 8. We find a rather good agreement between both methods. As in our case $Z(\pi,0)>Z(\pi/2,\pi/2)$ for all considered values of J/t. At small values of J $(0.01\leqslant J/t\leqslant0.5)$ SCBA finds a scaling of $Z(\pi/2,\pi/2)=0.31J^{2/3}$ and $Z(\pi,0)=0.35J^{0.7}$. For $J/t\geqslant1$, the results from SCBA overestimates the quasiparticle weight at the two considered k points, with an increasing deviation for larger values of J/t. Based on the quantitative agreement of SCBA with our results for small J, we can confidently conclude that the quasiparticle at $\vec{k}=(0,\pi)$ and $(\pi/2,\pi/2)$ should be finite for all values of J in the physically relevant region (i.e., $J/t\gtrsim0.1$).

As mentioned in the introduction, there are exact results for the quasiparticle weight at the supersymmetric point in two dimensions.[13] On the one hand, $Z(\vec{k}=0)=1/2$, a requirement that is fulfilled by our simulation, where the Green's function at that particular k point consists of a single exponential. In contrast to this, the estimate of SCBA is approximately 0.45 and that of VMC$\approx$0.32. Furthermore, Sorella showed that $Z(\vec{Q})/Z(0)\leqslant(2m)^2$, where $m^2=S(\vec{Q})/N$, $S(\vec{Q})$ being the magnetic structure factor at the antiferromagnetic wave vector. The equality is reached in the thermodynamic limit. Figure 9 shows the evolution with system size of $Z(\vec{Q})$ together with results from exact diagonalization for a 4×4 system and $(2m)^2\simeq0.37$ for $L\rightarrow\infty$. Although large error bars show that the determination of $Z(\vec{k})$ is less satisfactory for $\vec{k}=\vec{Q}$ than at $\vec{k}=(\pi/2,\pi/2)$, the data are consistent with the exact result. It was further suggested[13] that if $Z(\vec{k}+\vec{Q})/Z(\vec{k})=(2m)^2$ is satisfied for $\vec{k}\neq0$, a jump in the quasiparticle weight should be observed on crossing the border of the magnetic zone. Figure 10 shows $Z(\vec{k})$ along the symmetry directions in the Brillouin zone for a 24×24 system and $J/t=2$. Our data do not show any sizable jump. Unfortunately, it is not possible to consider arbitrarily long

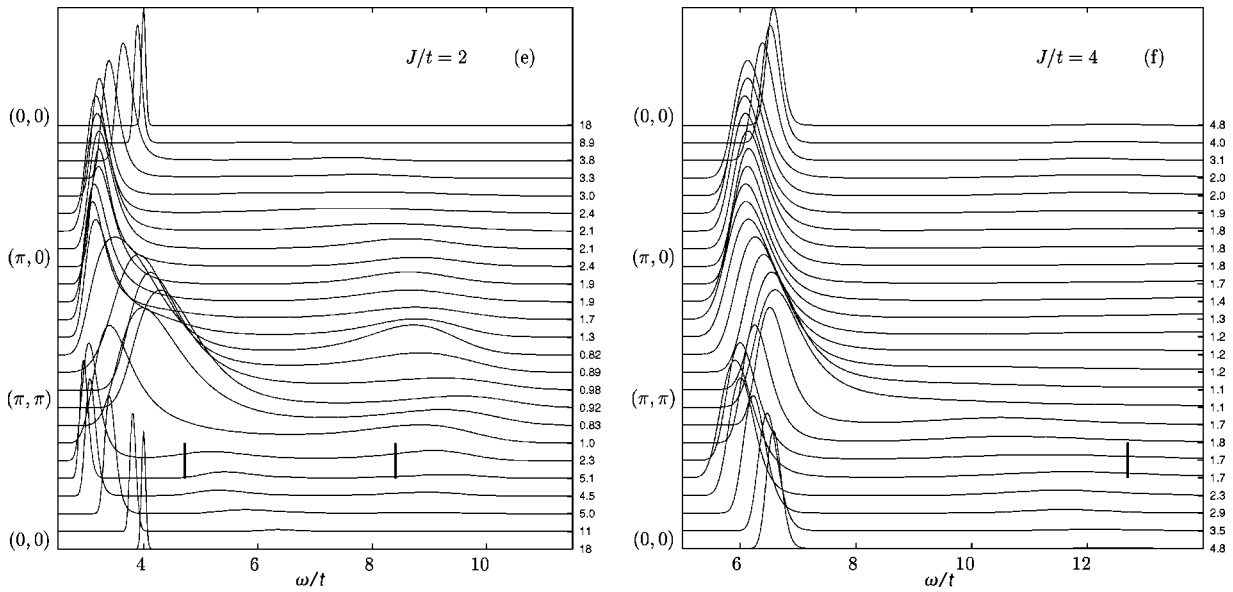

FIG. 11. (*Continued*).

imaginary times since as Eq. (11) shows, the errors are amplified exponentially. Therefore, our results cannot be considered as a proof of continuity. However, in view of the good agreement with the above-mentioned exact results, we consider them as a convincing evidence.

C. Spectral function and string excitations

The results discussed in Sec. III A for the lower edge of the spectrum and in Sec. III B for the quasiparticle weight can be recognized in the spectral function (Fig. 11) obtained by using MaxEnt. For clarity, the maximum of each curve is normalized to 1 in the plots. The small numbers on the right hand side of the figures correspond to the maximal value of $A(\vec{k},\omega)$ when the integral $\int_{-\infty}^{\infty} d\omega\, A(\vec{k},\omega)$ is properly normalized to $\pi/2$. The lower edge of the spectrum remains like in the previous section, but the accuracy of its location in $A(\vec{k},\omega)$ is reduced by MaxEnt. The peaks around $(0,\pi)$ and $(\pi/2,\pi/2)$ are generally very sharp, in agreement with the fact that a finite quasiparticle weight was found in Sec. III B. A transfer of weight from high to low energies can be observed, when J/t is increased, consistent with the increase in the quasiparticle weight (Fig. 7 in Sec. III B).

When compared to the one-dimensional (1D) case,[34] it is seen that the high-energy excitations in the 2D case are extremely broad. The total bandwidth remains essentially constant as a function of J in contrast to the 1D case, where it scales as $4t+J$.

For values of the coupling in the range $J/t \leqslant 2$ we observe satellite peaks in the region around $\vec{k}=(\pi/2,\pi/2)$ (Fig. 11) next to the lowest energy peak, which is extremely sharp and corresponds to a quasiparticle. The δ peak cannot be handled satisfactorily by MaxEnt. As can be seen by comparison of Figs. 2 and 11, MaxEnt gives some weight at energies lower than the band edge. This additional weight has to be balanced in some way, such that this error propagates to the other side of the δ peak. Small peaks in the vicinity of the δ peak, therefore, cannot be resolved. In order to resolve structures close to the quasiparticle peak, we subtract the exponential corresponding to the lowest energy (see Fig. 12). The thus modified Green's function can now be used as input of MaxEnt.

Before proceeding to the results, let us remark that, when the MaxEnt results obtained with the modified Green's function, i.e., after the subtraction of the lowest exponential, are viewed closely, on occasions, an additional peak appears at the bottom of the spectrum [this effect can be seen, e.g., for $(\pi/2,\pi/2)$ in Fig. 13]. To exclude, that this peak corresponds to a real physical effect, we take several modified Green's functions, that are consistent with the exponential of the lowest peak, within the statistical error. Therefore, we take the lowest and the highest exponential, that are consistent with the results obtained in Sec. III A, and use them as input of MaxEnt. As can be seen in Fig. 14, the new peak that appears below the low-energy peak of the original function, and hence is artificial, is only observed in two cases with varying position, whereas the two other peaks can be always observed, no matter which exponential is subtracted (always within the statistical errors). The position of these high-energy peaks is not changed by the different subtractions, only the width is affected. In all cases discussed, a small shift of these structures can be observed with respect to the ones in the spectrum without the subtraction. However, the positions assumed by these structures after the subtraction is not affected by the different subtractions within the values allowed by the statistical errors. We conclude that the initial

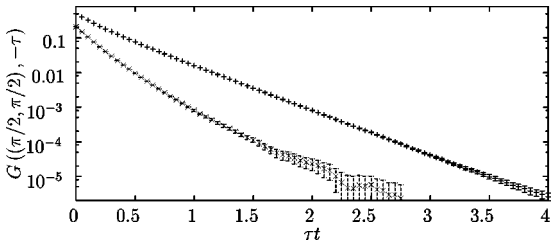

FIG. 12. Original Green's function and Green's function with subtraction (lower curve) for a 16×16 system and $J/t=2$ at $\vec{k}=(\pi/2,\pi/2)$.

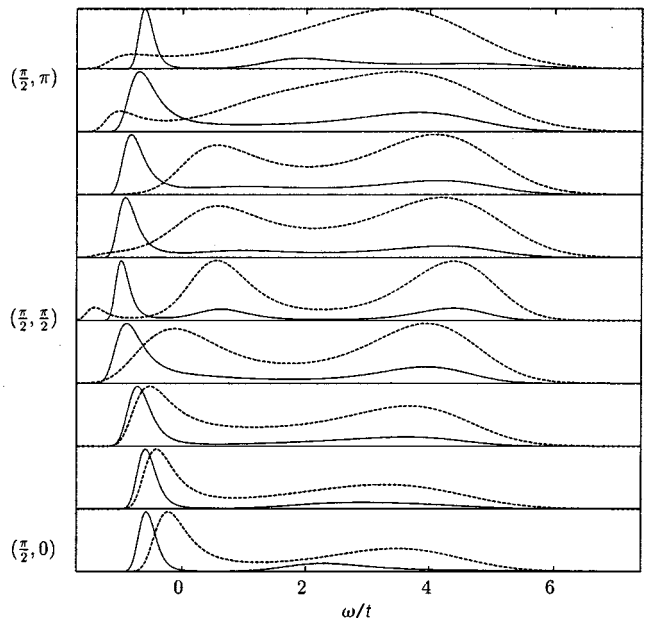

FIG. 13. Original spectrum (full line) and after subtraction (dashed line) along the line $(\pi/2,k_y)$. In the direction toward $(\pi/2,0)$ the lowest resonance approaches the position of the quasiparticle peak and merges with it, whereas toward $(\pi/2,\pi)$ the distance stays approximately constant. In the second case, the main effect is a broadening of the resonances. Shown is a 16×16 system with $J/t=0.6$.

small shift is due to the inability of MaxEnt to concentrate the weight of the delta function of the quasiparticle peak to a single energy value.

The result of the procedure described above is shown in Fig. 15. For $(\pi/2,\pi/2)$ there are only little changes of the position of the maxima of the existing peaks at small J/t compared to the full spectral function (except the low-energy peak, that disappeared). We can further observe, that the satellite peak next to the low-energy peak can now be seen for all values of $J/t\leqslant2$. One should notice, that no additional weight has been produced at high energies, but the normalization has changed (again the maximal value is normalized to 1, not the area of the spectral function).

At $(\pi/2,\pi/2)$ [Fig. 15(a)] the resolution of the second-lowest excitation is quite clear, when applying the above method, whereas at $(\pi,0)$ [Fig. 15(b)] the results are either not accurate enough, or the corresponding excitation is weaker. For $J/t=1.2$ the resolution is not good enough to separate the two resonances at $(\pi,0)$. Generally the excitations at higher energies at $(\pi,0)$ are broader than at $(\pi/2,\pi/2)$, so that the positions of the maxima are not as well defined. Similar structures were observed in exact diagonalization[8,7] and in SCBA,[12] and were ascribed to string excitations.

When the string picture is valid, as it is expected in the t-J_z model the hole is confined by a linear potential, leading to (k independent) eigenvalues of the energy[23,12,35] given by

$$E_n/t=-2\sqrt{3}+a_n(J_z/t)^{2/3}, \tag{12}$$

where a_n are the eigenvalues of a dimensionless Airy equation.[10] The first three eigenvalues are given by $a_n=2.33$, 4.08, and 5.52. In Fig. 16 the results for the first three

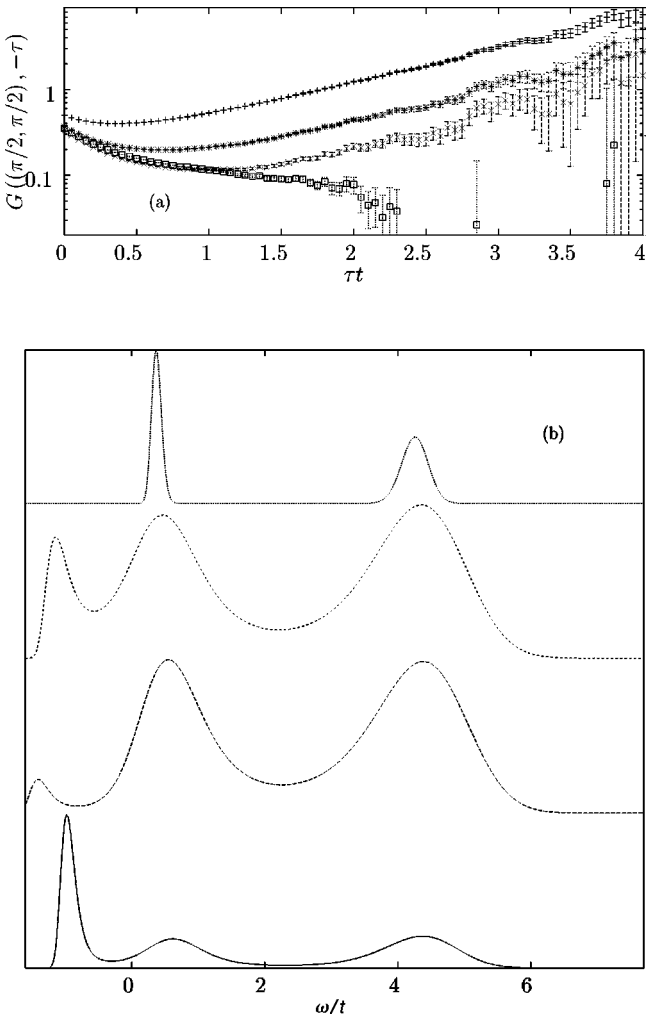

FIG. 14. Green's function and resulting spectral function before and after subtraction of the lowest exponential: $Z(\vec{k})\exp[-\epsilon(\vec{k}\tau)]$ on a 16×16 lattice, $J/t=0.6$, and $\vec{k}=(\pi/2,\pi/2)$. We estimate $Z(\vec{k})=0.176\pm0.025$ and $\epsilon(\vec{k})=-0.90\pm0.03$ (see Sec. III A). In (a) we show the original Green's function (top curve), and results when subtracting the exponentials corresponding to the values $\epsilon(\vec{k})=(-0.90-0.03)t$, $\epsilon(\vec{k})=-0.90t$, and $\epsilon(\vec{k})=(-0.90+0.03)t$. The MaxEnt results in (b) correspond (from bottom to top) the original spectral function, and to the results for $\epsilon(\vec{k})=-0.90t$, $(-0.90-0.03)t$, and $(-0.90+0.03)t$, respectively. For Fig. 15, we subtract the exponential $Z(\vec{k})\exp[-\epsilon(\vec{k})\tau]$, and consider the mean values of $Z(\vec{k})$ and $\epsilon(\vec{k})$.

excitations are given for $\vec{k}=(\pi/2,\pi/2)$, and are compared to the predictions from SCBA. The error bars on the second and third peak are obtained as the width of the MaxEnt peak at half intensity, the error bars of the first peak are taken as in Sec. III A. We find, that for $J/t\leqslant2$ the lowest peak can be accurately described by $\epsilon_0(\pi/2,\pi/2)=-E_H-3.28t+2.33(J/t)^{2/3}t$, where E_H is the Heisenberg energy per site, and the second peak by $\epsilon_1(\pi/2,\pi/2)=-E_H-3.28t+4.08(J/t)^{2/3}t$. The value of $3.28t+E_H$ is the result obtained from SCBA,[12] whereas the prefactors of $(J/t)^{2/3}$ are exactly the values of the dimensionless Airy function, implying that the first two peaks behave (within our error bars) exactly as it is expected by the string picture. In contrast to this, a fit from SCBA for the first three excitations in the t-J

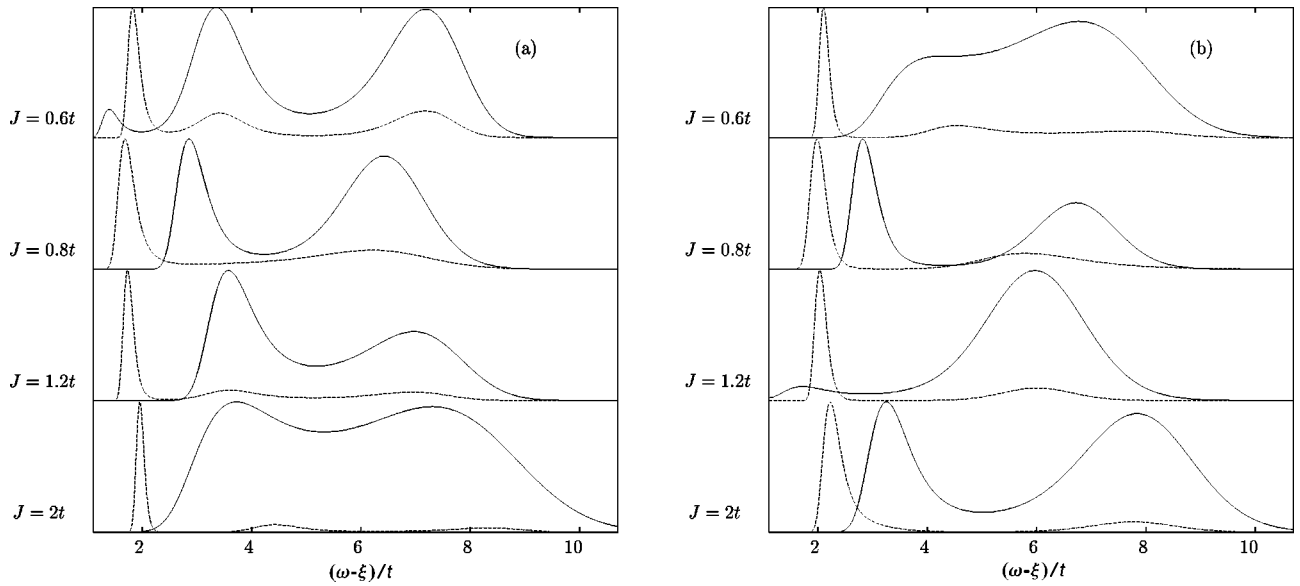

FIG. 15. Change of the spectral function when subtracting the first excitation for (a) $(\pi/2,\pi/2)$ and (b) $(\pi,0)$. The energy is shifted by an arbitrary amount ξ ($\xi=-2.8t,-2t,-t,+t$ for $J/t=0.6,0.8,1.2,2$, respectively), in order to display the spectra for different values of J/t in the same energy range. The dotted line is the original result, the full line gives the modified one.

model for values of $J/t\leqslant 0.4$, results in $a_n=2.16$, 5.46, and 7.81, also with the exponent 2/3,[12] leading to a clear disagreement with our data. The third peak that can be resolved cannot be explained by the string picture, since its distance to the lower band edge is independent of J and has a value of about $4t$. The existence of a string excitation is not restricted to $(\pi/2,\pi/2)$, but it can also be observed between $(\pi/2,\pi/2)$ and $(\pi/2,3\pi/4)$. This is demonstrated for the value $J/t=0.6$ (see Fig. 13).

The results above lead to the conclusion that the lowest excitations can be well described by the string picture. However, it should be kept in mind that the string picture originates in the Ising limit for $J/t\ll 1$, and that it is based on the continuum limit, that seems far away from our case with strings of lengths between two and a maximum of five lattice points, that correspond to the first two string excitations. Moreover, the string picture predicts a band without dispersion, that is clearly not the case in our simulations. A way to reconcile this paradoxical situation is given by the very good quantitative agreement between QMC and series expansions[21] for the dispersion of the quasiparticle and its bandwidth for a fairly large range in J. As shown by the expansion around the Ising limit, a coherent motion of the hole is made possible after the creation of strings due to hopping processes, by appropriate spin flips, the shortest string being of length two. The lowest-order contribution appears in third order, where the points $(\pi/2,\pi/2)$ and $(\pi,0)$ are degenerate. Fourth and higher-order processes remove this degeneracy, giving rise to a band that agrees qualitatively very well with the one obtained in QMC. Therefore on top of the coherent motion determined by $J_\perp$, stringlike excitations are possible and related to J_z and t. Such a possibility was already proposed by Béran, Poilblanc, and Laughlin (BPL)[32] on the basis of exact diagonalizations on small systems and is confirmed unambiguously by our simulations on large systems.

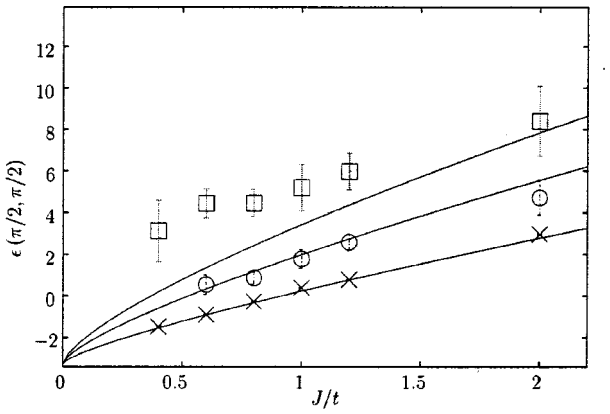

FIG. 16. The first three excitations at $\vec{k}=(\pi/2,\pi/2)$. At $J/t=0.4$ only two peaks were resolved. The lines represent the solutions obtained by solving the linear string potential for the hole in the t-J_z model.

At $J/t\gtrsim 2$ the excitations fall below the values predicted by the string picture. In those regions the string picture is no longer valid, as the relaxation of the disturbed spin bonds is faster than the motion of the hole.

IV. CONCLUSIONS

A new QMC algorithm was presented that allows a rather accurate determination of the single-hole dynamics in a two-dimensional Heisenberg $S-1/2$ antiferromagnet. The main advantages of this algorithm are the combination of the loop algorithm for the update of the spins and the exact evolution of the hole for a given spin configuration. Due to the diverging correlation length at zero temperature, large autocorrelation times should be expected for algorithms with local updates, a problem that is avoided here by the global update of the spins. On the other hand, the exact evolution of the hole for a given spin background avoids further statistical errors that would be introduced if the hole is updated stochastically,

as in recently proposed approaches.[26,27] In fact, the accuracy achieved allows for a determination of several dynamical quantities on large lattice sizes, leading to the possibility of a finite-size scaling of, e.g., the quasiparticle weight.

First (Sec. III A) we discussed the lower edge of the spectrum that is obtained directly from the asymptotics in imaginary time of the Green's function. This quantity is accessible to different techniques, that are however, with the exception of GFMC, either restricted to small lattice sizes or approximate. The comparison shows that very accurate results are given by series expansions over a large range of parameters, supporting thus the interpretation of the relevant physical processes for the coherent motion of the hole in the frame of a perturbative expansion around the Ising limit. This picture is further enforced by our study of the quasiparticle weight (Sec. III B) and the spectral function (Sec. III C). In Sec. III B it was shown, that indeed the lower edge of the spectrum describes the coherent propagation of a hole with finite quasiparticle weight. This is the case for all the parameter ranges studied, and due to the good agreement with SCBA, especially for small values of J, one can conclude that this coherent propagation takes place for essentially $J>0$. Furthermore, by considering structures next to the lowest peak in the spectral function (Sec. III C), it is seen that the lowest excitations around the wave vector $\vec{k}=(\pi/2,\pi/2)$ are very well described by the levels of strings usually discussed for the t-J_z model, giving further support to the perturbative picture, where the hole creates strings during its motion through the lattice, that are healed by exchange processes, leading thus to coherence. In fact, the strings for the first two levels, that agree quantitatively with our simulations, correspond to a length of two and five lattice sites. Strings of length two are the dominant contributions in series expansions for the dispersion of the quasiparticle. Moreover, our findings showing the existence of string resonances above the quasiparticle pole lend support to a picture developed by BPL,[32] where the composite nature of the quasiparticle is advanced. In previous exact diagonalization studies, the existence of such resonances, that were first observed in 4×4 lattices[33] were not clearly identified on larger lattices.[8] We have shown in Sec. III C that they can be quantitatively identified with string excitations. However, they are visible only in a rather narrow region along the line $k_x\simeq\pi/2$, $\pi/2\lesssim k_y\lesssim 3\pi/4$, such that in small lattices with up to 26 sites, these features can be very much affected by boundary effects. Following BPL, the quasiparticle can be viewed as a light holon attached to a spinon by a confining potential, the one that gives rise to the spectrum of string excitations.

A comparison with experiments[14–16] fails due to the small gap between the lowest peak at $\vec{k}=(\pi/2,\pi/2)$ and the flat band around $\vec{k}=(\pi,0)$. It was suggested by several authors[15,18,19] that this shift might be obtained introducing hopping terms to second and third nearest neighbors. Furthermore, it was found in exact diagonalizations[19] that such extra terms lead to a noticeable reduction of the quasiparticle weight. Since exact diagonalizations with second and third nearest neighbors in lattices with 18 and 26 sites suffer considerably under finite-size effects, a discussion of the influence of longer range hopping on the quasiparticle weight must be carried out in much larger lattices. Such studies are presently under way.

ACKNOWLEDGMENTS

This work was supported by Sonderforschungsbereich 382. The numerical calculations were performed at HLRS Stuttgart. The authors thank the above institutions for their support. We are grateful to P. Horsch, E. Manousakis, D. Poilblanc, P. Prevlošek, and S. Sorella for helpful and instructive discussions, and to CECAM, where part of these discussions took place, for its hospitality.

[1] W. F. Brinkman and T. M. Rice, Phys. Rev. B **2**, 1324 (1970).
[2] G. J. Bednorz and K. A. Müller, Z. Phys. B: Condens. Matter **64**, 188 (1986).
[3] P. W. Anderson, Science **235**, 1196 (1987); Phys. Rev. Lett. **64**, 1839 (1990).
[4] W. Metzner, P. Schmidt, and D. Vollhardt, Phys. Rev. B **45**, 2237 (1992).
[5] S. A. Trugman, Phys. Rev. B **37**, 1597 (1988).
[6] Q. F. Zhong and S. Sorella, Phys. Rev. B **51**, 16 135 (1995).
[7] E. Dagotto, Rev. Mod. Phys. **66**, 763 (1994).
[8] D. Poilblanc, H. Schulz, and T. Ziman, Phys. Rev. B **47**, 3268 (1993).
[9] S. Sorella, Phys. Rev. B **46**, 11 670 (1992).
[10] C. L. Kane, P. A. Lee, and N. Read, Phys. Rev. B **39**, 6880 (1989).
[11] G. Martinez and P. Horsch, Phys. Rev. B **44**, 317 (1991).
[12] Z. Liu and E. Manousakis, Phys. Rev. B **45**, 2425 (1992).
[13] S. Sorella, Phys. Rev. B **53**, 15 119 (1996).
[14] B. O. Wells, Z.-X. Shen, D. M. King, M. H. Kastner, M. Greven, and R. J. Birgenau, Phys. Rev. Lett. **74**, 964 (1995); S. LaRosa I. Vobornik, F. Zwick, H. Berger, M. Grioni, G. Margaritondo, R. J. Kelley, M. Onellion, and A. Chubukov, Phys. Rev. B **56**, R525 (1997).
[15] C. Kim, P. J. White, Z.-X. Shen, T. Tohyama, Y. Shibata, S. Maekawa, B. O. Wells, Y. J. Kim, R. J. Birgenau, and M. A. Kastner, Phys. Rev. Lett. **80**, 4245 (1998).
[16] F. Ronning, C. Kim, D. L. Feng, D. S. Marshall, A. G. Loeser, L. L. Miller, J. N. Eckstein, I. Borovic, and Z.-X. Shen, Science **282**, 2067 (1998).
[17] D. S. Marshall, D. S. Dessau, A. G. Loeser, L.-H. Park, A. Y. Matsuura, J. N. Eckstein, I. Borovic, P. Fournier, A. Kapitulnik, W. E. Spicer, and Z.-X. Shen, Phys. Rev. Lett. **76**, 4841 (1996).
[18] T. Tohyama, Y. Shibata, S. Maekawa, Z.-X. Shen, and N. Nagaosa, J. Phys. Soc. Jpn. **69**, 9 (2000).
[19] G. B. Martins, R. Eder, and E. Dagotto, Phys. Rev. B **60**, R3716 (1999).
[20] H. G. Evertz, M. Marcu, and G. Lana, Phys. Rev. Lett. **70**, 875 (1993); H. G. Evertz, cond-mat/9707221 (unpublished).
[21] C. J. Hamer, Z. Weihong, and J. Otimaa, Phys. Rev. B **58**, 15 508 (1998).
[22] M. Jarrell and J. Gubernatis, Phys. Rep. **269**, 133 (1996).
[23] L. N. Bulaevskii, Zh. Éksp. Theor. Fiz. 54, 1562 (1968) [JETP

27, 836 (1968)]; B. Shraiman and E. Siggia, Phys. Rev. Lett. **60**, 740 (1988).
[24] F. Zhang and T. M. Rice, Phys. Rev. B **37**, 3759 (1988).
[25] G. Khaliullin, Pis'ma Zh. Éksp. Teor. Fiz. **52**, 999 (1990) [JETP Lett. **52**, 389 (1990)]; A. Angelucci, Phys. Rev. B **51**, 11 580 (1995).
[26] N. V. Prokof'ev, B. V. Svistunov, and I. S. Tupitsyn, Zh. Éksp. Teor. Fiz. 114, 570 (1998) [JETP **87**, 310 (1998)].
[27] R. Brower, S. Chandrasekharan, and U.-J. Wiese, Physica A **3-4**, 520 (1998).
[28] B. B. Beard and U.-J. Wiese, Phys. Rev. Lett. **77**, 1865 (1996).
[29] M. Boninsegni and E. Manousakis, Phys. Rev. B **45**, 4877 (1992).
[30] M. Boninsegni, Phys. Lett. A **188**, 330 (1994).
[31] R. Eder and K. W. Becker, Z. Phys. B: Condens. Matter **78**, 219 (1990).
[32] P. Béran, D. Poilblanc, and R. B. Laughlin, Nucl. Phys. B **473**, 707 (1996).
[33] E. Dagotto, R. Joynt, S. Bacci, and E. Gagliano, Phys. Rev. B **41**, 9049 (1990).
[34] M. Brunner, F. F. Assaad, and A. Muramatsu, Eur. Phys. J. B **16**, 209 (2000).
[35] V. Elser, D. Huse, B. Shraiman, and E. Siggia, Phys. Rev. B **41**, 6715 (1990).